Nanoscale

RSC Publishing

PAPER

View Article Online
View Journal | View Issue

Cite this: *Nanoscale*, 2013, **5**, 8202

Efficient hybrid solar cells using PbS_xSe_{1-x} quantum dots and nanorods for broad-range photon absorption and well-assembled charge transfer networks†

Minwoo Nam,‡[a] Sungwoo Kim,‡[b] Sejin Kim,[b] Sang-Wook Kim*[b] and Keekeun Lee*[a]

Received 17th April 2013
Accepted 11th June 2013

DOI: 10.1039/c3nr01923c

www.rsc.org/nanoscale

We present hybrid solar cells with high efficiency utilizing a novel donor–acceptor combination of poly [2,6-(4,4′-bis-(2-ethylhexyl)dithieno[3,2-*b*:2′,3′-*d*]silole)-*alt*-4,7(2,1,3-benzothiadiazole)] (PSBTBT) and a PbS_xSe_{1-x} inorganic semiconductor. Several nanocomposite parameters are evaluated in order to improve the hybrid device efficiency, including donor–acceptor materials, surface modification of the inorganic semiconductor, and mixture of quantum dots (QDs) and nanorods (NRs) in the polymer matrix. A high power conversion efficiency (PCE) of ~3.4% is attained from the optimal device with a $PbS_{0.7}Se_{0.3}$ QD : NR blending ratio of 0.3 : 0.7 (wt/wt) under air mass (AM) 1.5 solar illumination, which is attributed to the broad-range absorption of the solar energies and the efficient charge separation and transport dynamics. The optoelectronic and nanomorphological properties of these novel hybrid solar cells are described.

Introduction

Hybrid bulk heterojunction solar cells, which comprise inorganic semiconductor nanocrystals (NCs) in a conjugated polymer matrix, have attracted much attention due to the film-forming properties of polymers[1] and the unique properties of NCs, such as the quantum confinement effect[2] and multiple exciton generation.[3] The lifetimes of photoinduced polarons can be increased by ~10 times when NCs are employed as electron acceptors in place of the organic fullerene derivatives, denoting great promise of hybrid systems for exceeding the performance of their organic counterparts.[4] Until now, a number of attempts have been made to improve the efficiency of hybrid solar cells by changing various parameters such as the type of NC or polymer materials used,[4,5] the size and shape of NCs,[6,7] the overall thickness of hybrid nanocomposites,[8] the concentration ratio of NCs in a polymer matrix,[8,9] or the type of heterojunction.[10,11] The state of the art of hybrid solar cells is well described in recent review papers.[12,13] S. Ren *et al.*[14] reported a hybrid solar cell utilizing efficient electronic interactions by binding CdS quantum dots (QDs) onto crystalline poly(3-hexylthiophene) (P3HT) nanorods (NRs). Bicontinuous donor–acceptor (D–A) phases and a well-defined interface in the hybrid blend provide the power conversion efficiency (PCE) of ~4.1%, which is the highest value in hybrid bulk heterojunction solar cells up to now, suggesting that controlling phase separation and improving interfacial areas of QDs and polymers are very important. J. Seo *et al.*[15] employed near-infrared (NIR)-sensitive PbS QDs and a new kind of low-bandgap polymer to form a favorable type-II heterojunction and to achieve a broad spectral response from UV to NIR regions, and demonstrated that in their hybrid nanocomposites, the size of QDs largely affects photovoltaic performances and relatively small PbS QDs (first exciton peak at 915 nm) show a high PCE value of 3.78%. However, even though such progress is quite inspiring, the state-of-the-art efficiencies in hybrid solar cells are merely less than ~10.6% for purely organic devices[16,17] or ~7.4% for purely inorganic NC devices.[18] The most limiting factors for these low efficiencies are considered to be poor combinations of the two heterogeneous materials of inorganic NCs and organic polymers. For example, phase separation at interfacial areas of NCs and polymer results in poor dissociation of photogenerated excitons, and discontinuous percolation networks impede the efficient transport of charge carriers at their corresponding phases. Several recent studies addressed these issues by incorporating 1-D nanomaterials in polymer matrices as a means of enhancing exciton dissociation and charge-transport, which includes blends of spherical QDs and elongated NRs of CdSe,[19] selectively N- or B-doped carbon nanotubes (CNTs),[20] and hybrid nanomaterials by binding InP QDs along N-doped CNT surfaces.[21]

In this study, we introduce novel hybrid bulk heterojunction solar cells that incorporate efficient interfacial areas between QDs and polymer matrices and provide high efficiency. Fig. 1 shows a schematic view of the developed device structure and

[a]*Department of Electrical and Computer Engineering, Ajou University, Woncheon-dong, Yeongtong-gu, Suwon 443-749, Republic of Korea. E-mail: keekeun@ajou.ac.kr; Tel: +82-31-219-1848*

[b]*Department of Molecular Science and Technology, Ajou University, Woncheon-dong, Yeongtong-gu, Suwon 443-749, Republic of Korea. E-mail: swkim@ajou.ac.kr; Tel: +82-31-219-2522*

† Electronic supplementary information (ESI) available. See DOI: 10.1039/c3nr01923c

‡ These two authors have equally contributed to this study.

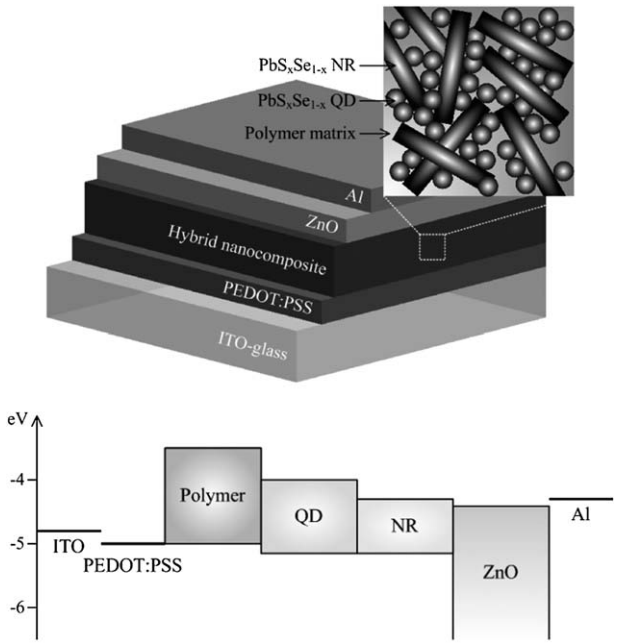

Fig. 1 Schematic view of the hybrid bulk heterojunction solar cell and its corresponding energy band diagram. The device comprises sequential layers of ITO-coated glass, PEDOT:PSS, hybrid nanocomposites (PSBTBT:QDs and NRs), ZnO, and Al. Both QDs and NRs are embedded in a low-bandgap polymer matrix with a total polymer-to-inorganic semiconductor ratio of 1 : 9. The HOMO and LUMO levels of the PSBTBT were taken from ref. 23. The E_C and E_V levels of the QDs and NRs were determined from CV measurements.

corresponding energy band diagram. The hybrid nanocomposite is based on a new D–A combination of poly[2,6-(4,4′-bis-(2-ethylhexyl)dithieno[3,2-*b*:2′,3′-*d*]silole)-*alt*-4,7(2,1,3-benzothiadiazole)] (PSBTBT) as an electron donor and QDs and NRs of ternary PbS_xSe_{1-x} semiconductor as electron acceptors simultaneously. PSBTBT is a new kind of low-bandgap polymer with an optimal bandgap of 1.4 eV and high crystallinity, which can contribute to a better match with the solar spectrum, broader exploitation of the solar energy, and well organized nanomorphology compared to those of other typical polymers such as P3HT.[22–24] When illuminated by solar light, both the polymer and the inorganic semiconductors absorb photon energies to produce charge carriers over a wide range of the solar spectrum across the UV-NIR regions. Owing to the two inorganic NC elements with large interfacial areas, photogenerated electron–hole pairs have a high probability of separation at D–A interfacial boundaries, followed by the efficient transport of electrons *via* the straight pathways within NRs that are continuously interconnected by QDs.[19,21] The devices developed were characterized by changing various parameters, including the polymer and NC materials, the surface ligand modification of NCs, the blending ratio of QDs : NRs in the polymer matrices, and the hybrid nanocomposite layer thickness.

Experimental section

Synthesis of PbS_xSe_{1-x} QDs

For the synthesis of QDs, lead(II) acetate trihydrate (0.25 mmol) and oleic acid (1 mmol) were mixed in a 25 ml flask. The solution was degassed under vacuum with a pressure of 10^{-5} Torr at 100 °C for 2 h. After cooling to room temperature, 4 ml of diphenyl ether were added to the solution, which was degassed at 65 °C for 30 min and heated to 150 °C under a nitrogen atmosphere. Then, 0.1 mmol of tri-*n*-octylphosphine–bis-(trimethylsilyl)sulfide (TOP–TMS) solution was rapidly injected, and the mixture was maintained at 120 °C for 30 min. Subsequently, the QDs were precipitated with ethanol. The S : Se ratio in the ternary PbS_xSe_{1-x} system (0.7 : 0.3 and 0.9 : 0.1 for example) was controlled by systematically varying the amount of S in the precursor ratio, as demonstrated elsewhere.[28]

Synthesis of PbS_xSe_{1-x} NRs

In the case of NRs, lead(II) acetate trihydrate (0.25 mmol), hexadecylamine (0.5 mmol), and oleic acid (1.25 mmol) were mixed in a three-neck flask. The mixture was heated to 110 °C and degassed under vacuum (10^{-5} Torr) for 2 h. Then, 4 ml of diphenyl ether were added to the reaction flask at room temperature, after which the temperature was heated to 65 °C and maintained under vacuum (10^{-5} Torr) for 30 min. The precursor solution was prepared by mixing tri-*n*-octylphosphine (TOP)–Se (0.07 mmol) and bis(trimethylsilyl)sulfide (0.03 mmol) in 1 ml of TOP solvent. The flask was then heated to 150 °C under nitrogen (10^{-5} Torr). At this temperature, the precursor solution was rapidly injected, and the mixture was maintained at 120 °C for 30 min. After the reaction, the nanocrystals were precipitated with ethanol. To separate the QDs and NRs, size-selective precipitation was carried out in a hexane–methanol solvent system.

Device fabrication

Fig. 2 shows the fabrication process of the hybrid bulk heterojunction solar cell. To perform the solution-based fabrication processes, the prepared QDs and NRs were blended in chlorobenzene with desired ratios (wt/wt). PSBTBT dissolved in chlorobenzene was directly introduced into a solution that contained

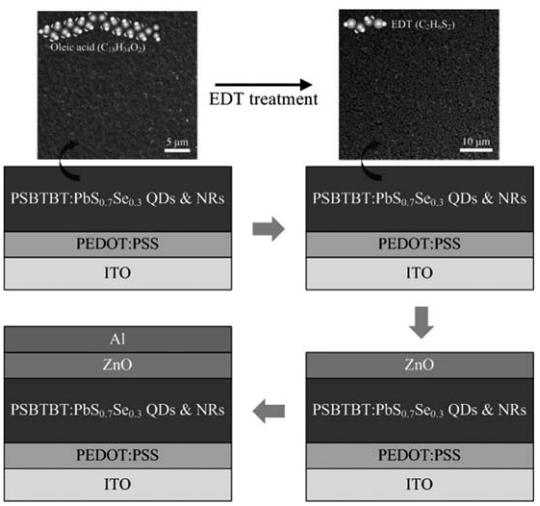

Fig. 2 Fabrication process of the hybrid bulk heterojunction solar cell.

both QDs and NRs with a total polymer-to-NC (QDs and NRs) ratio of 1 : 9 (wt/wt). PEDOT:PSS was first spin-coated onto a glass substrate with pre-patterned ITO electrodes, and then dried at 120 °C for 10 min. The hybrid solution was fully intermixed through ultrasonication and spin-coated on top of the PEDOT:PSS layer. Post-chemical treatment was performed in ambient air to exchange the pre-formed OA with an end-functional group. Several drops of 0.01 M EDT solution in acetonitrile were poured onto the hybrid blend film, followed by spin coating for 20 s. The film was then rinsed with pure acetonitrile and chlorobenzene sequentially to remove free-standing molecules, and then stored in a glove box filled with nitrogen. A morphological change in the hybrid blends after EDT treatment is observed in scanning electron microscopy (SEM) images. Then, ZnO nanoparticles (NPs) prepared from zinc acetate dehydrate (demonstrated elsewhere) were dispersed in acetone (15 mg ml^{-1}) and spin-coated on top of the photo-active layer to form the 40 nm thick electron-transporting and hole-blocking layer.[25,26] An Al electrode was evaporated onto the ZnO layer through a shadow mask under high vacuum conditions with a pressure of $\sim10^{-6}$ Torr. The device was annealed at 150 °C for 20 min under a nitrogen atmosphere. The device is ultimately composed of sequential layers of ITO-glass, PEDOT:PSS (35 nm), a hybrid photoactive layer (~110 nm), ZnO (40 nm), and Al (100 nm). An active area of 0.04 cm^{-2} was defined as the overlap between the top and bottom electrodes.

Characterization

TEM images were taken to examine the shape and size of the prepared QDs and NRs using a Tecnai G2 F30 S-Twin FE-TEM (FEI) with an accelerating voltage of 300 kV. Crystal structures of the NCs were characterized using an Ultima III high-resolution diffractometer (Rigaku) equipped with a rotating anode and a Cu-Kα radiation source. Optical absorbance and PL spectra of the QDs and NRs separately dispersed in TCE were observed using a V-670 UV-vis-NIR spectrophotometer (JASCO) and a USB-4000 spectrofluorometer (Ocean Optics), respectively. The thickness of the polymer:NC (1 : 9 wt/wt) hybrid films was evaluated using a NanoMap-500LS contact surface profilometer (AEP). The TRPL intensity measurement was carried out with a time-correlated single photon counting (TCSPC) system using EasyLife LS (PTI). A pulsed laser of 375 nm was used for excitation, and appropriate filters for each case were employed. Optical absorbance spectra of the hybrid films were monitored using a Cary 5000 UV-vis-NIR spectrophotometer (Varian). Surface morphology variations of the films after EDT treatment were detected using a JSM-6700F FE-SEM (JEOL). The samples for detecting cross-sectional microscopic images were prepared by focused ion-beam (FIB) machining, in which a Nova 600 NanoLab (FEI) equipped with an SEM was used. Cross-sectional TEM images and EDS scanning were obtained using a JEM-2100F (JEOL). The film samples for these measurements were prepared on a pre-cleaned bare glass slide using the spin-coating technique and then annealed at 150 °C for 30 min in ambient air. The *J–V* characteristics of the developed devices were measured using a source meter (Keithley 2400) in the dark and under AM 1.5G illumination. White light was provided by a 450 W Xe lamp (Oriel) equipped with an AM 1.5G filter as a solar simulator. The intensity of 100 mW cm^{-2} was calibrated using a reference Si diode without considering a spectral mismatch factor. EQE spectra were measured using a 300 W Xe light source and a monochromator provided by a Polaronix K3100 IPCE measurement system (McScience). The photovoltaic performance measurements were performed in ambient air immediately after fabrication.

Results and discussion

Characterization of ternary $PbS_{0.7}Se_{0.3}$ QDs and NRs

Details for the synthesis process of $PbS_{0.7}Se_{0.3}$ QDs and NRs can be found in the Experimental section and in our previous work.[27] Fig. 3a and b show transmission electron microscopy (TEM) images of the prepared QDs and NRs, respectively. The size and shape of QDs and NRs are highly uniform. The mean diameter of the 0-D spherical QDs is ~4 nm, which is small enough to take advantage of the quantum size effect. The 1-dimensional NRs showed a similar diameter of ~4 nm, but had an elongated length of 30–40 nm with an aspect ratio of ~10.

Fig. 3c shows the X-ray diffraction (XRD) spectra of the alloyed QDs and NRs, and bulk PbSe and PbS peaks are

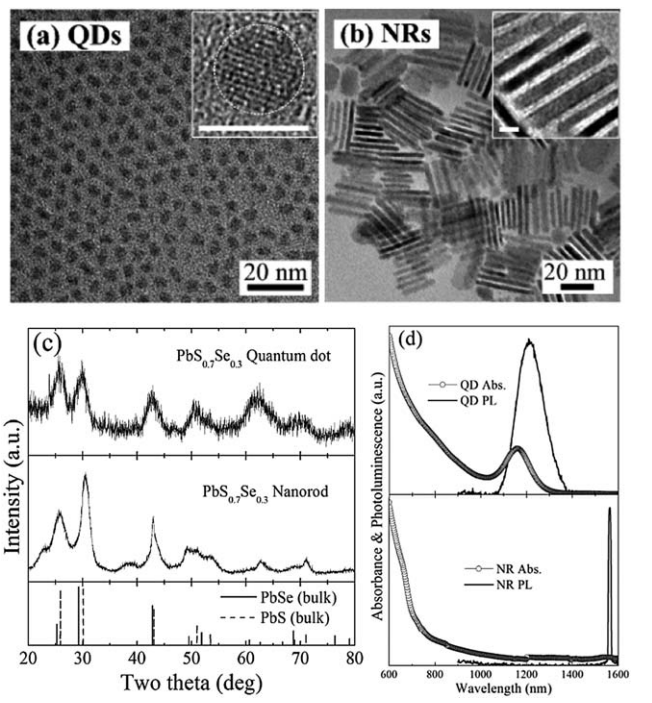

Fig. 3 TEM images of the as-synthesized $PbS_{0.7}S_{0.3}$ inorganic semiconductors with two different shapes: (a) QDs and (b) NRs. The scale bars in the insets are 5 nm. (c) XRD spectra of the two elements and reference diagrams for bulk PbS and PbSe. The peaks from the ternary QDs and NRs are accurately positioned between the individual peaks of the binary semiconductors, indicating the successfully alloyed ternary NCs. (d) Vis-NIR absorbance and PL spectra of the QDs and NRs. For the measurement, the as-synthesized QDs and NRs were separately dispersed in TCE.

presented as references. The peaks from our ternary $PbS_{0.7}Se_{0.3}$ NCs were precisely positioned between the peaks of the binary compounds PbSe and PbS. W. Ma *et al.*[28] reported that the difference in the atomic anion radii is less than 15% and the lattice mismatch factor is as small as 2% between PbS and PbSe. The similar properties of PbS and PbSe can lead to the successful preparation of the substitutional $PbS_{0.7}Se_{0.3}$ alloy.

Fig. 3d shows the optical absorbance and photoluminescence (PL) spectra of the QDs and NRs separately dispersed in trichloroethylene (TCE). Both broadband absorption profiles and emission peaks in NIR regions observed from both solutions imply the possibility of broad-ranging solar light exploitation ranging from the UV to NIR wavelengths. The weak absorbance peak from NRs is primarily due to non-uniformity in the morphology between NRs and their dense packing. In general, a QD sample with a much better mono-dispersity shows a stronger peak compared with a NR sample. The absorption and PL peaks of NRs were considerably red-shifted relative to those of QDs. This is because NCs of the Pb chalcogenide group tend to undergo significantly large changes in their bandgaps in accordance with their size, as a result of their large dielectric constants and consequently large exciton Bohr radii.[29] Based on the exciton absorption peaks, the optical bandgaps of the QDs and NRs were ~1.1 eV and ~0.8 eV, respectively, which were highly similar to the values obtained experimentally using cyclovoltammetry (CV) measurement, as shown in Fig. 1.

Optimization of hybrid devices using PbS_xSe_{1-x} QDs in a polymer matrix

To find an optimal D–A bulk heterojunction system, several donor and acceptor materials were assessed using simple devices, structured with an indium tin oxide (ITO, 180 nm)/poly(3,4-ethylenedioxythiophene) poly(styrenesulfonate) (PEDOT:PSS, 35 nm)/hybrid blend of QDs and polymer (~90 nm)/ZnO (40 nm)/Al (100 nm). Fig. 4a shows a photograph of the fabricated device and its cross-sectional SEM image, in which sequential layers are clearly discernible. In the hybrid blend, the blending ratio of PbS_xSe_{1-x} QDs and a polymer was 9 : 1 (wt/wt). PEDOT:PSS serves as a hole-transporting layer and smoothens the ITO surface,[12] while the ZnO layer serves as an electron-transporting layer, provides improved electrical contacts between the photoactive layer and Al, and works as an optical spacer.[25,30,31] The types of materials in the hybrid photoactive layer were confirmed based on energy dispersive spectroscopy (EDS) elemental analysis (see Fig. S1 in the ESI†).

Fig. 4b shows the current–voltage (*J*–*V*) characteristics of three devices with distinct D–A combinations under air mass (AM) 1.5 illumination. P3HT or PSBTBT was selectively used as an electron donor, while $PbS_{0.7}Se_{0.3}$ QDs or $PbS_{0.9}Se_{0.1}$ QDs were selectively used as electron acceptors. Based on the previous report,[28] S : Se ratios of 0.7 : 0.3 and 0.9 : 0.1 in the ternary system exhibit PCE values higher than those of other S : Se proportions, which is the reason why the two S : Se ratios were selectively compared. Post-ligand treatment was carried out on the hybrid blends for exchanging the pre-formed oleic acid (OA) ligands with end-functional 1,2-ethanedithiol (EDT) molecules, to ultimately modify the interfacial contacts of QDs and polymer matrices, and hence, to improve carrier transport efficiency.[32] Details of the ligand exchange procedure are described in the Experimental section.

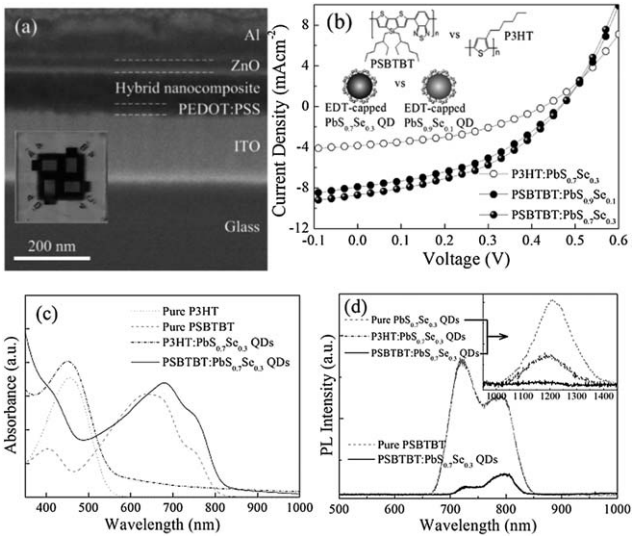

Fig. 4 (a) A photograph of the developed hybrid solar cell and its cross-sectional SEM image. Sequential layers of ITO (180 nm)-coated glass, PEDOT:PSS (35 nm), hybrid photoactive nanocomposite (~90 nm), ZnO (40 nm), and Al (100 nm) are clearly discernible. (b) *J*–*V* characteristics of the prototypical solar cells based on QD:polymer hybrid bulk heterojunction systems. Three devices with different kinds of donor or acceptor materials were prepared: P3HT:$PbS_{0.7}Se_{0.3}$ QDs, PSBTBT:$PbS_{0.7}Se_{0.3}$ QDs, and PSBTBT:$PbS_{0.9}Se_{0.1}$ QDs. Chemical structures of the two polymers and schematic view of the EDT-capped QDs are depicted. (c) Vis-NIR absorbance spectra of hybrid blends in the solution state, comprising $PbS_{0.7}Se_{0.3}$ QDs and either P3HT or PSBTBT. Absorbance spectra of the two pure polymers are also provided. (d) PL intensity spectra of pure PSBTBT and PSBTBT:$PbS_{0.7}S_{0.3}$ QD blend. The inset compares PL spectra of pure $PbS_{0.7}Se_{0.3}$ QDs and P3HT:$PbS_{0.7}Se_{0.3}$ QD blend, and PSBTBT:$PbS_{0.7}Se_{0.3}$ QD blend in the longer NIR wavelength region. These are to investigate dynamics of exciton dissociation and subsequent charge transfer between the polymer matrix and QDs.

The device using PSBTBT as an electron donor instead of the general conjugated polymer, P3HT, showed a significantly increased performance. As shown in Fig. 4c, the optimal optical bandgap of ~1.4 eV in PSBTBT provides not only a better match with the solar spectrum, but also broader exploitation of the solar spectrum extending to the NIR regions, as compared to the case of P3HT.[22] This broad-range photon harvesting led to high photocurrent values in the PSBTBT-based hybrid devices. Another advantage is the favorable photoinduced charge transfer between PSBTBT and the QDs, which was better than that between P3HT and the QDs. To clarify the assumption, PL quenching was measured using solution samples of pure PSBTBT and PSBTBT:$PbS_{0.7}Se_{0.3}$ QD blend, as shown in Fig. 4d. The PL was almost completely quenched by blending QDs into the PSBTBT solution, indicating highly efficient dynamics of exciton dissociation by the energy offset at the hybrid heterojunction and subsequent ultrafast electron transfer from PSBTBT to QDs before recombination. The inset in Fig. 4d compares PL spectra of pure $PbS_{0.7}Se_{0.3}$ QDs, a PSBTBT:QD blend, and a P3HT:$PbS_{0.7}Se_{0.3}$ QD blend in the longer NIR

wavelength region. The degree of PL quenching was significantly larger in the PSBTBT-based nanocomposite relative to that of the P3HT-based nanocomposite, which is a good indication of the better charge transfer between PSBTBT and $PbS_{0.7}Se_{0.3}$ QDs. It seems that there are insufficient energy differences between the lowest unoccupied molecular orbital (LUMO)/highest occupied molecular orbital (HOMO) levels of P3HT (3.2 eV/5.1 eV)[33] and conduction band (E_c)/valence band (E_v) levels of $PbS_{0.7}Se_{0.3}$ QDs (4.0 eV/5/15 eV), whereas PSBTBT has proper LUMO/HOMO levels of ~3.5 eV/~5.0 eV to form a more energetic type-II heterojunction.[23,34]

Regarding the effect of the S : Se alloy ratio in the ternary QDs, $PbS_{0.7}Se_{0.3}$ QDs tend to derive higher J_{SC} than $PbS_{0.9}Se_{0.1}$ QDs to produce a better PCE, while the V_{OC} and fill factor (FF) values are similar. In general, PbSe has better carrier transport efficiency than PbS in photovoltaic devices, but a lower optical bandgap, owing to the differences in intrinsic properties between the binary compounds.[35] Therefore, the decrease in J_{SC} with decreasing Se concentration in the alloy system can be analysed in the same context. This is consistent with the previous report by W. Ma *et al.*,[28] in which they demonstrated that the S : Se proportion in the ternary PbS_xSe_{1-x} system affects both the carrier transport and voltage in photovoltaic devices. Besides, they described that the S : Se ratio of 0.7 : 0.3 presents an overall efficiency higher than those of other ratios (*e.g.*, 0.9 : 0.1) as an optimal ratio in the ternary system.

Based on these findings, PSBTBT and $PbS_{0.7}Se_{0.3}$ QDs are proposed to be the optimal D–A combination for a bulk heterojunction. The performances obtained here are relatively higher than those of existing hybrid solar devices based on PbS(e) QDs, which is attributed to the favorable type-II heterojunctions in the novel D–A combination system. However, the performance is still as low as ~2%, and thus requires strategies to further improve efficiencies of the internal charge dissociation and subsequent transport. Therefore, we devised more efficient hybrid devices with increased interfacial areas, and improved the bicontinuous percolation networks by embedding both QDs and NRs together in PSBTBT, which resulted in dramatically increased PCEs.

Hybrid devices using both $PbS_{0.7}Se_{0.3}$ QDs and NRs in the PSBTBT matrix

To fabricate such hetero-structured devices, hybrid compounds with different blending ratios of QDs and NRs were prepared, while the total polymer-to-$PbS_{0.7}Se_{0.3}$ ratio (wt/wt) was maintained at 1 : 9. Fig. 5a shows the *J–V* characteristics of five devices with different blending ratios of QDs : NRs in the PSBTBT matrices. The device structure is the same as that shown in Fig. 4a, and the thickness of the photoactive film was controlled to 90–110 nm based on our experimental optimization (see Fig. S2 in the ESI†). Interestingly, all hetero-structured devices showed dramatically enhanced J_{SC} and FF compared to those based on a single NC element. Additionally, the V_{OC} values in the hetero-structured devices were not significantly decreased, despite supplementing an amount of NRs in the blends, while the polymer:NR only device showed a considerably lower V_{OC} due to the low-bandgap of the NRs. We believe that the electron transport improvement due to the mixture of NRs and QDs results in fewer space charges and thus higher built-in potential to prevent V_{OC} reduction.[8] Incorporating both QDs and NRs is thought to allow for the exploitation of the respective advantages of QDs and NRs and for surmounting the drawbacks of the two components. We postulate that the high efficiencies in the hetero-structured devices are due to the better exciton dissociation and carrier transport dynamics.

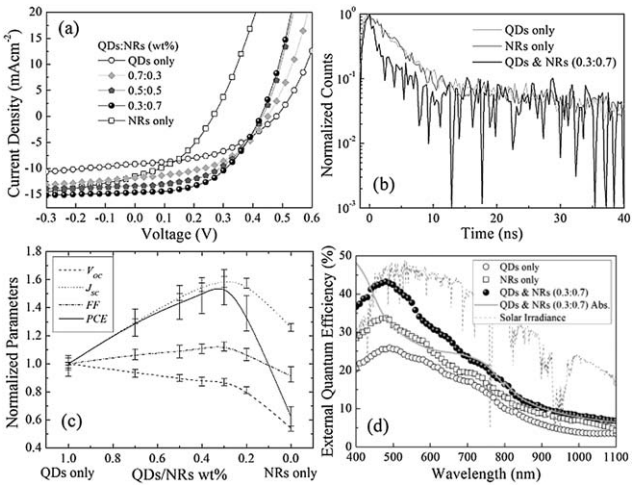

Fig. 5 (a) *J–V* characteristics of the hybrid solar cells with different blending ratios of QDs and NRs (wt/wt) in the PSBTBT matrix, while maintaining the total polymer-to-$PbS_{0.7}Se_{0.3}$ NC ratio at 1 : 9 (wt/wt). (b) TRPL spectra of the hybrid films with a thickness of ~110 nm. (c) Normalized photovoltaic performance parameters of J_{SC}, V_{OC}, FF, and PCE as a function of QD:NR blending ratio. The standard deviations are taken from 20 reliable data points among more than 30 devices. (d) EQE spectra of the three distinct devices with different inorganic semiconductor elements of QDs only, NRs only, and QDs:NRs (0.3 : 0.7).

To validate this assumption, Fig. 5b shows the normalized transition decay of the PL for the three differently composed nanocomposites. The PL lifetime (τ_1) of 0.056 ns for hetero-structured nanocomposites is considerably less than 0.168 ns for QDs only or 0.113 ns for NRs only. The time-resolved PL (TRPL) data from three separate measurements are summarized in Table S1 in the ESI.† The shortening of the PL lifetime signifies that photogenerated excitons become dissociated before emission at the enhanced interfacial contact, and that improved electron transport from organic to inorganic phases is energetically favored within the well-assembled hetero-structured networks.[36] Therefore, blending both QDs and NRs into the polymer matrices is believed to be a facile and effective method for converting absorbed photon energies into photocurrents.

Fig. 5c shows the normalized photovoltaic parameters as a function of the QD : NR blending ratio in the hybrid blends, arranged for ease of comparison. The highest PCE was attained when the QD : NR blending ratio was 0.3 : 0.7 (wt/wt), resulting from the higher J_{SC} and FF. The optimal heterostructure contains a relatively high amount (wt%) of NRs. We infer that there is a large amount of QDs in the blend, given the small and

light-weight characteristics of QDs (even though the total amount of QDs is numerically only 30%). As a result, the optimal blend can take advantage of not only the large carrier dissociation interfaces at QDs with a high surface area-to-volume ratio but also the straight carrier pathways within NRs that are conductively bridged by small QDs.

Among more than 30 devices developed under the same conditions, the best PCE of 3.4% was accomplished with a V_{OC} of 0.43 V, J_{SC} of 14.87 mA cm^{-2}, and FF of 0.53. To the best of our knowledge, the photocurrent density in this study is considerably higher than those of other NIR hybrid solar cells, which includes the world record value recently reported by J. Seo *et al.*[15] Table 1 compares the photovoltaic performance parameters in this study and extracted from ref. 15. The low V_{OC} relative to the "E_g − 0.6 V" upper limit for common bulk heterojunction devices reduces the overall efficiency,[5] albeit to a range similar to that of the highest PCE thus far.

Fig. 5d shows the external quantum efficiency (EQE) spectra of the three devices with different inorganic semiconductor components. Both the EQE spectra and spectral responses of the film after EDT treatment look similar, implying combined contributions of the polymer (at 500–900 nm) and the NIR-sensitizing inorganic semiconductor to photocurrent generation. The J_{SC} values calculated from the EQE spectra are similar to those obtained from *J*–*V* curves within the measurement error. For example, the J_{SC} of the hetero-structured device was 14.02 mA cm^{-2} based on the EQE spectrum, which is only 4% smaller than the measured J_{SC} value. The tendencies in EQE spectra between the samples confirm again that the hetero-structured blend allows for better internal charge dissociation and transport. This is because EQE is theoretically determined by the products of the successive steps of photon absorption, photogenerated exciton diffusion, exciton separation, carrier transport, and charge collection at the electrodes.[37] In the optimal device, more than 20% of the photocurrent is generated by low-energy photons in the NIR regions based on simple integration: $\int_{800nm}^{1100nm} EQE(\lambda)d\lambda \Big/ \int_{400nm}^{1100nm} EQE(\lambda)d\lambda$. Therefore, the device is assumed to convert photons with low energies into electricity successfully.

To gain further insight into the nanoscale distribution geometries, Fig. 6a and b show the plane and cross-sectional TEM images of the hetero-structured blend, respectively. Interactive networks of QDs and NRs in PSBTBT were clearly observed without severe aggregations between the elements, indicating that interpenetrating networks are formed in both the horizontal and perpendicular directions of the film. The distribution geometry was dissimilar to those of blends with a single NC element of QDs or NRs alone. For example, the polymer:NR only blend showed huge NR–NR clusters that impede charge carrier generation over the entirety of the hybrid film (see Fig. S3 in the ESI†). Therefore, it is believed that the small-sized QDs in the hetero-structured nanocomposite not only serve as conductive links at voids between NRs but also prevent agglomeration of the elongated NRs.

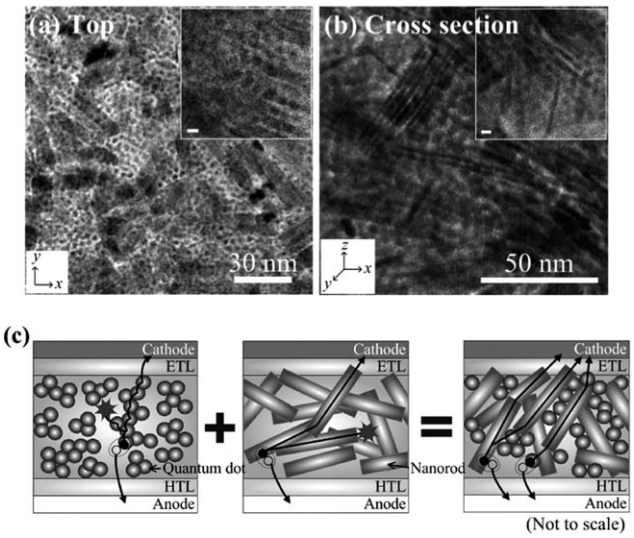

Fig. 6 TEM images of the hybrid blend with QDs and NRs (0.3 : 0.7 wt/wt) in the PSBTBT matrix: (a) top and (b) cross-sectional views. The scale bars in the insets are 5 nm. Continuous interfacial contacts by both QDs and NRs are clearly shown in both horizontal and perpendicular directions of the film. (c) Cross-sectional schematic diagram of the three differently composed devices to explain the superiority of the hetero-structured blends. Electron transport in the polymer:QD blends is mainly dependent on hopping events. Polymer:NR only blends provide direct pathways for more efficient electron transport, but suffer from voids and horizontal aggregations of the elongated NRs. In the QD:NR intermixtures, 1-D NRs provide direct pathways, and 0-D QDs fill the voids between NRs for charge separation and electron transport dynamics. ETL and HTL represent the electron-transporting layer and hole-transporting layer, respectively.

Fig. 6c summarizes the superiorities of the hetero-structured blends based on our experimental results. Devices based on QDs in the polymer suffer from poor charge transport efficiency, presumably due to recombinations during frequent carrier hopping events, as well as charge traps at "dead ends" in the blend.[38] For hybrid nanocomposites using NRs instead of QDs, charge generation cannot evenly occur inside all the NR inner phases, because of the tendencies of 1-D NRs to agglomerate between them and to lie horizontally in the plane of the film.[39] Additionally, a significant reduction of the optical bandgap due to the quantum size effect decreases V_{OC}, resulting in reduction of the overall efficiency. In contrast, in hybrid nanocomposites including both QDs and NRs in the polymer matrix, the NRs furnish direct carrier transport routes along the rods for efficient transport of the photogenerated carriers with minimized carrier hopping, while QDs are located at void sites between the

Table 1 Comparison of the photovoltaic parameters presented in this study and extracted from the recent paper[a]

	V_{OC} (V)	J_{SC} (mA cm^{-2})	FF	PCE (%)
PSBTBT:$PbS_{0.7}Se_{0.3}$ QDs and NRs (avg)	0.42	14.61	0.52	3.19
PSBTBT:$PbS_{0.7}Se_{0.3}$ QDs and NRs (best)	0.43	14.87	0.53	3.40
PDTPBT:PbS QDs[15]	0.57	13.06	0.51	3.78

[a] PDTPBT is poly(2,6-(*N*-(1-octylnonyl)dithieno[3,2-*b*:20,30-*d*]pyrrole)-*alt*-4,7-(2,1,3-benzothiadiazole)).

elongated NRs, deterring the agglomeration tendency of NRs as well as acting as continuous conductive links. Continuous, well-assembled charge separation and transport dynamics are obtained by simultaneously employing two kinds of inorganic materials with different dimensions and shapes. Additionally, the interfacial contacts between inorganic nanomaterials and polymer are improved by modifying the QD and NR surfaces through manipulation treatment of the ligand length. These are the main reasons for the high photovoltaic performance in the hetero-structured devices investigated. We believe that controlling the nanomorphology of the blends, such as by arranging NRs vertically, further increases the performance.[37,40]

Conclusions

We have developed hybrid bulk heterojunction solar cells based on a new D–A combination of $PbS_{0.7}Se_{0.3}$ NCs and a low-bandgap polymer PSBTBT. Incorporating both QDs and NRs of $PbS_{0.7}Se_{0.3}$ in the polymer matrix resulted in better performance than devices using either QDs or NRs alone, owing to the straight pathways for photogenerated carriers within NRs that are conductively interconnected by spherical QDs. In the optimal device, ultrafast exciton dissociation, energetic electron transport within well-assembled percolation networks, and broad-ranging exploitation of solar energy extending to the NIR regions led us to attain a high efficiency of 3.4%.

Acknowledgements

This work was supported by the Priority Research Centers Program (2012-0006687), Republic of Korea.

Notes and references

1 S. Günes, K. P. Fritz, H. Neugebauer, N. S. Sariciftci, S. Kumar and G. D. Scholes, *Sol. Energy Mater. Sol. Cells*, 2007, **91**, 420.
2 A. P. Alivisatos, *Science*, 1996, **271**, 933.
3 J. B. Sambur, T. Novet and B. A. Parkinson, *Science*, 2010, **330**, 63.
4 K. M. Noone, S. Subramaniyan, Q. Zhang, G. Cao, S. A. Jenekhe and D. S. Ginger, *J. Phys. Chem. C*, 2011, **115**, 24403.
5 K. M. Noone, E. Strein, N. C. Anderson, P.-T. Wu, S. A. Jenekhe and D. S. Ginger, *Nano Lett.*, 2010, **10**, 2635.
6 J. Yang, A. Tang, R. Zhou and J. Xe, *Sol. Energy Mater. Sol. Cells*, 2011, **95**, 476.
7 S. Dayal, M. O. Reese, A. J. Ferguson, D. S. Ginley, G. Rumbles and N. Kopidakis, *Adv. Funct. Mater.*, 2010, **20**, 2629.
8 Y. Zhou, M. Eck, C. Men, F. Rauscher, P. Niyamakom, S. Yilmaz, I. Dumsch, S. Allard, U. Scherf and M. Krüger, *Sol. Energy Mater. Sol. Cells*, 2011, **95**, 1232.
9 C.-Y. Liu, Z. C. Holman and U. R. Kortshagen, *Nano Lett.*, 2009, **9**, 449.
10 Y. Zhang, Z. Li, J. Ouyang, S.-W. Tsang, J. Lu, K. Yu, J. Ding and Y. Tao, *Org. Electron.*, 2012, **13**, 2773.
11 M. Nam, S. Kim, M. Kang, S.-W. Kim and K.-K. Lee, *Org. Electron.*, 2012, **13**, 1546.
12 J. Chandrasekaran, D. Nithyaprakash, K. B. Ajjan, S. Maruthamuthu, D. Manoharan and S. Kumar, *Renewable Sustainable Energy Rev.*, 2011, **15**, 1228.
13 B. R. Saunders, *J. Colloid Interface Sci.*, 2012, **369**, 1.
14 S. Ren, L.-Y. Chang, S.-K. Lim, J. Zhao, M. Smith, N. Zhao, V. Bulovic, M. Bawendi and S. Gradecak, *Nano Lett.*, 2011, **11**, 3998.
15 J. Seo, M. J. Cho, D. Lee, A. N. Cartwright and P. N. Prasad, *Adv. Mater.*, 2011, **23**, 3984.
16 G. Li, R. Zhu and Y. Yang, *Nat. Photonics*, 2012, **6**, 153.
17 http://www.nrel.gov/ncpv/images/efficiency_chart.jpg.
18 A. H. Ip, S. M. Thon, S. Hoogland, O. Voznyy, D. Zhitomirsky, R. Debnath, L. Levina, L. R. Rollny, G. H. Carey, A. Fischer, K. W. Kemp, I. J. Kramer, Z. Ning, A. L. Labelle, K. W. Chou, A. Amassian and E. H. Sargent, *Nat. Nanotechnol.*, 2012, **7**, 577.
19 K. F. Jeltsch, M. Schädel, J.-B. Bonekamp, P. Niyamakom, F. Rauscher, H. W. A. Lademann, I. Dumsch, S. Allard, U. Scherf and K. Meerholz, *Adv. Funct. Mater.*, 2012, **22**, 397.
20 J. M. Lee, J. S. Park, S. H. Lee, H. Kim, S. Yoo and S. O. Kim, *Adv. Mater.*, 2011, **23**, 629.
21 J. M. Lee, B.-H. Kwon, H. I. Park, H. Kim, M. G. Kim, J. S. Park, E. S. Kim, S. Yoo, D. Y. Jeon and S. O. Kim, *Adv. Mater.*, 2013, **25**, 2011.
22 B. A. Collins, Z. Li, C. R. McNeill and H. Ade, *Macromolecules*, 2011, **44**, 9747.
23 S. Sista, M.-H. Park, Z. Hong, Y. Wu, J. Hou, W. L. Kwan, G. Li and Y. Yang, *Adv. Mater.*, 2010, **22**, 380.
24 H. Lu, B. Akgun and T. P. Russell, *Adv. Energy Mater.*, 2011, **1**, 870.
25 J. Gilot, I. Barbu, M. M. Wienk and R. A. J. Janssen, *Appl. Phys. Lett.*, 2007, **91**, 113520.
26 C. Pacholski, A. Kornowski and H. Weller, *Angew. Chem., Int. Ed.*, 2002, **41**, 1188.
27 M. Nam, S. Kim, T. Kim, S.-W. Kim and K.-K. Lee, *Appl. Phys. Lett.*, 2011, **99**, 233115.
28 W. Ma, J. M. Luther, H. Zheng, Y. Wu and A. P. Alivisatos, *Nano Lett.*, 2009, **9**, 1699.
29 F. W. Wise, *Acc. Chem. Res.*, 2000, **33**, 773.
30 J. J. Choi, Y.-F. Lim, M. B. Santiago-Berrios, M. Oh, B.-R. Hyun, L. Sun, A. C. Bartnik, A. Goedhart, G. G. Malliaras, H. D. Abruña, F. W. Wise and T. Hanrath, *Nano Lett.*, 2009, **9**, 3749.
31 J. Y. Kim, S. Noh, D. Lee, P. K. Nayak, Y. Hong and C. Lee, *J. Nanosci. Nanotechnol.*, 2011, **11**, 5995.
32 E. J. D. Klem, D. D. MacNeil, P. W. Cyr, L. Levina and E. H. Sargent, *Appl. Phys. Lett.*, 2007, **90**, 183113.
33 J. Y. Kim, K. Lee, N. E. Coates, D. Moses, T.-Q. Nguyen, M. Dante and A. J. Heeger, *Science*, 2007, **317**, 222.
34 J. Hou, H.-Y. Chen, S. Zhang, G. Li and Y. Yang, *J. Am. Chem. Soc.*, 2008, **130**, 16144.
35 J. M. Luther, M. Law, M. C. Beard, Q. Song, M. O. Reese, R. J. Ellingson and A. J. Nozik, *Nano Lett.*, 2008, **8**, 3488.

36 J. Seo, S. J. Kim, W. J. Kim, R. Singh, M. Samoc, A. N. Carywright and P. N. Prasad, *Nanotechnology*, 2009, **20**, 0952021.
37 B. R. Saunders and M. L. Turner, *Adv. Colloid Interface Sci.*, 2008, **138**, 1.
38 M. Skompska, *Synth. Met.*, 2010, **160**, 1.
39 J. C. Hindson, Z. Saghi, J. Hernandez-Garrido, P. A. Midgley and N. C. Greenham, *Nano Lett.*, 2011, **11**, 904.
40 J. Liu, S. Wang, Z. Bian, M. Shan and C. Huang, *Appl. Phys. Lett.*, 2009, **94**, 173107.